A Geometric Approach to Strapdown Magnetometer Calibration in Sensor Frame ⋆

J.F. Vasconcelos * **G. Elkaim** ** **C. Silvestre** * **P. Oliveira** * **B. Cardeira** *

* *Institute for Systems and Robotics (ISR), Instituto Superior Técnico, Lisbon, Portugal. Tel:351-21-8418054, Fax:351-21-8418291. e-mail: {jfvasconcelos, cjs, pjcro, bcardeira}@isr.ist.utl.pt*
** *Department of Computer Engineering, University of California SantaCruz, 1156 High St., SantaCruz, CA, 95064. e-mail:elkaim@soe.ucsc.edu*

Abstract: In this work a new algorithm is derived for the onboard calibration of three-axis strapdown magnetometers. The proposed calibration method is written in the sensor frame, and compensates for the combined effect of all linear time-invariant distortions, namely soft iron, hard iron, sensor non-orthogonality, bias, among others. A Maximum Likelihood Estimator (MLE) is formulated to iteratively find the optimal calibration parameters that best fit to the onboard sensor readings, without requiring external attitude references. It is shown that the proposed calibration technique is equivalent to the estimation of an ellipsoidal surface, and that the sensor alignment matrix is given by the solution of the orthogonal Procrustes problem. Good initial conditions for the iterative algorithm are obtained by a suboptimal batch least squares computation. Simulation and experimental results with low-cost sensors data are presented, supporting the application of the algorithm to autonomous vehicles and other robotic platforms.

1. INTRODUCTION

Magnetometers are a key aiding sensor for attitude estimation in low-cost, high performance navigation systems (Humphreys et al., 2005; Choukroun et al., 2004), with widespread application to autonomous air, ground and ocean vehicles. These inexpensive, low power sensors allow for accurate attitude aiding by comparing the magnetic field vector observation in body coordinates with the vector representation in Earth coordinates (Markley, 1989).

Magnetometer readings are subject to magnetic distortions and nonideal sensor effects which hinder the sensor usability and motivate several calibration techniques found in the literature. The classic compass swinging proposed in (Bowditch, 1984) is a heading calibration algorithm that computes scalar parameters using a least squares algorithm, but requires external heading information (Gebre-Egziabher et al., 2006). A methodology to calibrate the soft and hard iron parameters in heading and pitch resorting only to the magnetic compass data is found in (Denne, 1979). Although the derivation of the algorithm is mathematically sound, it is obtained by means of successive approximations and in a deterministic fashion that does not exploit the redundancy of multiple compass readings.

In recent literature, advanced magnetometer calibration algorithms have been proposed to tackle distortions such as bias, hard iron, soft iron and non-orthogonality directly in the sensor space, with no external attitude references and using optimality criteria. The batch least squares calibration algorithm derived in (Elkaim and Foster, 2006; Gebre-Egziabher et al., 2006) accounts for non-orthogonality, scaling and bias errors. A nonlinear, two-step estimator provides the initial conditions using a nonlinear change of variables to cast the calibration in a pseudo-linear least squares form. The obtained estimate of the calibration parameters is then iteratively processed by a linearized least squares batch algorithm.

The TWOSTEP batch method proposed in (Alonso and Shuster, 2002) is based on the observations of the differences between the norms of the modeled and the measured vectors, denoted as scalar-checking. In the first step of the algorithm, the centering approximation suggested by (Gambhir, 1975) produces a good initial guess of the calibration parameters, by rewriting the calibration problem in a linear least squares form. In a second step, a batch Gauss-Newton method is adopted to iteratively estimate the bias, scaling and non-orthogonality parameters. In related work, (Crassidis et al., 2005) derives recursive algorithms for magnetometer calibration based on the centering approximation and on nonlinear Kalman filtering techniques.

Magnetic errors such as soft iron, hard iron, scaling, bias and non-orthogonality are modeled separately in (Elkaim and Foster, 2006; Gebre-Egziabher et al., 2006). Although additional magnetic transformations can be modeled, it is known that some sensor errors are compensated by an equivalent effect, e.g. the hard iron and sensor biases are grouped together in (Gebre-Egziabher et al., 2006). Therefore, the calibration procedure should address the

⋆ This work was partially supported by Fundação para a Ciência e a Tecnologia (ISR/IST plurianual funding) through the POS Conhecimento Program that includes FEDER funds and by the project PTDC/EEA-ACR/72853/2006 HELICIM. The work of J.F. Vasconcelos was supported by a PhD Student Scholarship, SFRH/BD/18954/2004, from the Portuguese FCT POCTI programme.

estimation of the joint effect of the sensor errors, as opposed to estimating each effect separately.

In this work, the magnetometer reading error model is discussed and formulated to account for the combined effect of modeled and unmodeled linear time-invariant magnetic transformations. It is shown that the calibration problem is equivalent to that of estimating the parameters of an ellipsoid manifold, and a Maximum Likelihood Estimator (MLE) is formulated to find the best estimate of the calibration parameters using the sensor readings. A closed form solution for the magnetometer alignment is also presented, based on the well known solution to the orthogonal Procrustes problem (Gower and Dijksterhuis, 2004). The calibration and alignment methodology is formulated in the sensor frame, without resorting to external information or models about the magnetic field.

To the best of the authors' knowledge, this work is an original rigorous derivation of a calibration algorithm using a comprehensive model of the sensor readings in $\mathbb{R}^3$, that clarifies and exploits the geometric locus of the magnetometer readings, given by an ellipsoid manifold. It is also shown that the calibration and alignment procedures are distinct.

The proposed calibration methodology is assessed both in simulation and using experimental data. The calibration parameters are estimated for magnetometer data collected in ring shaped sets, corresponding to yaw and pitch maneuvers that are feasible for most land, air and ocean vehicles in common operational scenarios.

This paper is organized as follows. In Section 2, a unified magnetometer error parametrization is derived and formulated. It is shown that the calibration parameters describe an ellipsoid surface and that the calibration and alignment problems are distinct. A MLE formulation is proposed to calculate the optimal generic calibration parameters and an algorithm to provide good initial conditions is presented. Also, a closed form solution for the magnetometer alignment problem is obtained. Simulation and experimental results obtained with a low-cost magnetometer triad are presented and discussed in Section 3. Finally, Section 4 draws concluding remarks and comments on future work.

NOMENCLATURE

The notation adopted is fairly standard. The set of $n \times m$ matrices with real entries is denoted as $\mathrm{M}(n,m)$ and $\mathrm{M}(n) := \mathrm{M}(n,n)$. The sets of diagonal, positive diagonal, orthogonal, and special orthogonal matrices are respectively denoted by $\mathrm{D}(n)$, $\mathrm{D}^+(n) = \{\mathbf{S} \in \mathrm{D}(n) : \mathbf{S} > 0\}$, $\mathrm{O}(n) := \{\mathbf{U} \in \mathrm{M}(n) : \mathbf{U}'\mathbf{U} = \mathbf{I}\}$, $\mathrm{SO}(n) := \{\mathbf{R} \in \mathrm{O}(n) : \det(\mathbf{R}) = 1\}$. The n-dimensional sphere and ellipsoid are respectively described by $\mathrm{S}(n) = \{\mathbf{x} \in \mathbb{R}^{n+1} : \|\mathbf{x}\|^2 = 1\}$ and $\mathrm{L}(n) = \{\mathbf{x} \in \mathbb{R}^{n+1} : \|\mathbf{S}\mathcal{R}'\mathbf{x}\|^2 = 1\}$, where $\mathbf{S} \in \mathrm{D}^+(n+1)$ and $\mathcal{R} \in \mathrm{SO}(n+1)$ describe the radii and orientation of the ellipsoid, respectively.

2. MAGNETOMETER CALIBRATION AND ALIGNMENT

In this section, the magnetometer errors are characterized and a unified sensor reading model is obtained, evidencing that the magnetometer measurements are contained in an ellipsoid manifold. The magnetometer calibration algorithm is derived using a Maximum Likelihood Estimator formulation to find the calibration parameters that maximize the likelihood of the sensor readings. An algorithm to provide a good initial guess of the calibration parameters is proposed, and a closed form optimal alignment determination method is also presented.

2.1 Magnetometer Errors Characterization

The magnetometer readings are distorted by the presence of ferromagnetic elements in the vicinity of the sensor, by the interference between the magnetic field and the vehicle structure, by local permanently magnetized materials, and by technological limitations of the sensor. A detailed description of magnetic distortions and sensor errors is found in (Denne, 1979; Gebre-Egziabher et al., 2006) and references therein.

The three-axis magnetometer reading is modeled as

$$\mathbf{h}_{r\,i} = \mathbf{S}_M \mathbf{C}_{NO}(\mathbf{C}_{SI}\, {}^{B}_{E}\mathbf{R}_i\, {}^{E}\mathbf{h} + \mathbf{b}_{HI}) + \mathbf{b}_M + \mathbf{n}_{m\,i} \quad (1)$$

where $\mathbf{h}_r$ is the magnetometer reading in the (non-orthogonal) magnetometer coordinate frame, $\mathbf{S}_M \in \mathrm{D}^+(3)$ and $\mathbf{b}_M \in \mathbb{R}^3$ represent the sensor scaling and bias, respectively, $\mathbf{C}_{NO}$ is the non-orthogonality transformation described in (Elkaim and Foster, 2006), $\mathbf{C}_{SI} \in \mathrm{M}(3)$ is the soft iron transformation matrix, $\mathbf{b}_{HI} \in \mathbb{R}^3$ is the hard iron bias, $\mathbf{n}_m \in \mathbb{R}^3$ is the Gaussian wideband noise, and $i = 1, \ldots, n$ denotes the index of the reading.

2.2 Magnetometer Error Parametrization

In this section, an equivalent error model for the magnetometer readings is formulated. It is shown that the non-ideal magnetic effects are equivalent to a rotation, scaling and translation transformation, and hence that the sensor can be calibrated by estimating the center, orientation and radii of the ellipsoid that best fit to the acquired data.

Without loss of generality, the magnetometer reading (1) can be rewritten as

$$\mathbf{h}_{r\,i} = \mathbf{C}\, {}^{B}\mathbf{h}_i + \mathbf{b} + \mathbf{n}_{m\,i} \quad (2)$$

where $\mathbf{C} = \mathbf{S}_M \mathbf{C}_{NO} \mathbf{C}_{SI}$, $\mathbf{b} = \mathbf{S}_M \mathbf{C}_{NO} \mathbf{b}_{HI} + \mathbf{b}_M$, ${}^{B}\mathbf{h}_i = {}^{B}_{E}\mathbf{R}_i\, {}^{E}\mathbf{h}$, ${}^{B}\mathbf{h}_i \in \mathrm{S}(2)$ is the magnetic field in body coordinate frame. In particular, $\mathbf{C} \in \mathrm{M}(3)$ and $\mathbf{b} \in \mathbb{R}^3$ are unconstrained, so unmodeled linear time-invariant magnetic errors and distortions are also taken into account.

Given that the points ${}^{B}\mathbf{h}_i$ are contained in the sphere, straightforward application of the Singular Value Decomposition (SVD) (Strang, 1988) shows that the magnetometer readings $\mathbf{h}_{r\,i}$ lie on an ellipsoid manifold, as illustrated in the example of Fig. 1 and summarized in the following theorem.

Theorem 1. (Strang (1988)). Let $c : \mathbb{R}^n \to \mathbb{R}^n, c(\mathbf{x}) = \mathbf{C}\mathbf{x}$ be a linear transformation where $\mathbf{C} \in \mathrm{M}(n)$ is full rank. Then $c(\mathbf{x})$ is a bijective transformation between the sphere and an ellipsoid in $\mathbb{R}^n$, i.e. there is an ellipsoid $\mathrm{L}(n-1)$ such that the transformation $c|_{\mathrm{S}} : \mathrm{S}(n-1) \to \mathrm{L}(n-1)$, $c|_{\mathrm{S}}(\mathbf{x}) = \mathbf{C}\mathbf{x}$ is bijective.

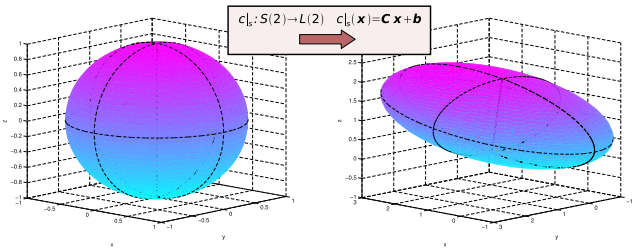

Fig. 1. Affine transformation of a two dimensional sphere

A direct result of Theorem 1 is that the sensor ellipsoid, centered at $\mathbf{b}$, is fully characterized by a rotation $\mathcal{R}_L$ and a scaling $\mathbf{S}_L$ matrices.

Corollary 1. Let $\mathbf{C} \in \mathrm{M}(n)$ be a full rank matrix and let the SVD decomposition of $\mathbf{C}$ be given by $\mathbf{C} = \mathcal{R}_L \mathbf{S}_L \mathbf{V}_L'$ where $\mathcal{R}_L \in \mathrm{SO}(n)$, $\mathbf{S}_L \in \mathrm{D}^+(n)$ and $\mathbf{V}_L \in \mathrm{O}(n)$. The ellipsoid described by $c|_S$ is spanned by the bijective transformation $l : \mathrm{S}(n-1) \to \mathrm{L}(n-1), \quad l(\mathbf{x}) = \mathcal{R}_L \mathbf{S}_L \mathbf{x}$.

Applying Corollary 1, the equivalent model for the magnetometer readings (2) is described by

$$\mathbf{h}_{r\,i} = \mathcal{R}_L \mathbf{S}_L {}^C\mathbf{h}_i + \mathbf{b} + \mathbf{n}_{m\,i} \tag{3}$$

where

$${}^C\mathbf{h}_i := \mathbf{V}_L' {}^B\mathbf{h}_i, \quad {}^C\mathbf{h}_i \in \mathrm{S}(2) \tag{4}$$

and $\{C\}$ denotes the calibration frame obtained by the orthogonal transformation $\mathbf{V}_L'$ of $\{B\}$. Clearly, the calibration process is equivalent to the estimation of the ellipsoid's parameters $\mathbf{b}$, $\mathcal{R}_L$ and $\mathbf{S}_L$ lying on the manifold $\Theta := \mathrm{SO}(3) \times \mathrm{D}^+(3) \times \mathbb{R}^3$. The alignment matrix $\mathbf{V}_L$ is implicit in ${}^C\mathbf{h}_i$, and hence can not be determined in the calibration process.

The sensor calibration and alignment algorithm is structured as follows. In the *calibration* step, the parameters $\mathcal{R}_L$, $\mathbf{S}_L$ and $\mathbf{b}$ are estimated, using a Maximum Likelihood Estimator formulated on M(3). In the *alignment* step, the determination of the orthogonal transformation $\mathbf{V}_L$ is obtained from a closed form optimal algorithm using vector readings in $\{C\}$ and $\{B\}$ frames.

2.3 Magnetometer Calibration

The calibration parameters are computed using a Maximum Likelihood Estimator. Assuming that the noise on the magnetometer readings is a zero mean Gaussian process with variance $\sigma^2_{m\,i}$, the probability density function (p.d.f.) of each $\mathbf{h}_{r\,i}$ is also Gaussian

$$\mathbf{n}_{m\,i} \sim \mathcal{N}(0, \sigma^2_{m\,i}\mathbf{I}) \Rightarrow \mathbf{h}_{r\,i} \sim \mathcal{N}(\mathcal{R}_L \mathbf{S}_L {}^C\mathbf{h}_i + \mathbf{b}, \sigma^2_{m\,i}\mathbf{I})$$

The MLE finds the parameters that maximize the conditional p.d.f. of each sensor reading given the optimization parameters (Kay, 1993). The resulting minimization problem of the weighted log-likelihood function is described by

$$\min_{\substack{(\mathcal{R}_L, \mathbf{S}_L, \mathbf{b}) \in \Theta \\ {}^C\mathbf{h}_i \in \mathrm{S}(2), i=1,\ldots,n}} \sum_{i=1}^{n} \frac{1}{\sigma^2_{m\,i}} \left\| (\mathbf{h}_{r\,i} - \mathbf{b}) - \mathcal{R}_L \mathbf{S}_L {}^C\mathbf{h}_i \right\|^2 \tag{5}$$

Solving the minimization problem (5) implies estimating n auxiliary magnetic field vectors ${}^C\mathbf{h}_i$, and the dimension of the search space is $(2n + \dim \Theta)$ whereas the dimension of the calibration parameters space is $\dim \Theta = \dim \mathrm{SO}(3) + \dim \mathrm{D}^+(3) + \dim \mathbb{R}^3 = 9$. To produce a computationally less intensive formulation, the minimization problem (5) is rewritten as

$$\min_{\substack{(\mathcal{R}_L, \mathbf{S}_L, \mathbf{b}) \in \Theta \\ {}^C\mathbf{h}_i \in \mathrm{S}(2), i=1,\ldots,n}} \sum_{i=1}^{n} \frac{1}{\sigma^2_{m\,i}} \| \mathbf{S}_L^{-1} \mathcal{R}_L' (\mathbf{h}_{r\,i} - \mathbf{b}) - {}^C\mathbf{h}_i \|^2 \tag{6}$$

which is suboptimal with respect to the unified error model (3), but can be rigorously derived using a MLE formulation by assuming that the noise is external to the sensor, as detailed in Appendix A. More important, the log-likelihood function (6) can be optimized by searching only in the parameter space Θ.

Proposition 2. The solution $(\mathcal{R}_L^*, \mathbf{S}_L^*, \mathbf{b}^*)$ of (6) also minimizes

$$\min_{(\mathcal{R}_L, \mathbf{S}_L, \mathbf{b}) \in \Theta} \sum_{i=1}^{n} \frac{1}{\sigma^2_{m\,i}} (\| \mathbf{S}_L^{-1} \mathcal{R}_L' (\mathbf{h}_{r\,i} - \mathbf{b}) \| - 1)^2 \tag{7}$$

Proof. Given $(\mathcal{R}_L^*, \mathbf{S}_L^*, \mathbf{b}^*)$, the optimal ${}^C\mathbf{h}_i^*$ satisfies

$${}^C\mathbf{h}_i^* = \underset{{}^C\mathbf{h}_i \in \mathrm{S}(2)}{\operatorname{argmin}} \| \mathbf{v}_i^* - {}^C\mathbf{h}_i \|^2 \tag{8}$$

where $\mathbf{v}_i^* := \mathbf{S}_L^{*-1} \mathcal{R}_L^{*\prime} (\mathbf{h}_{r\,i} - \mathbf{b}^*)$. The minimization problem (8) corresponds to the projection of $\mathbf{v}_i^*$ on the unit sphere, which has the closed form solution ${}^C\mathbf{h}_i^* = \frac{\mathbf{v}_i^*}{\|\mathbf{v}_i^*\|}$. Therefore, the minimization problem (6) can be written as $\min_{(\mathcal{R}_L, \mathbf{S}_L, \mathbf{b}) \in \Theta} \sum_{i=1}^{n} \frac{1}{\sigma^2_{m\,i}} \| \mathbf{S}_L^{-1} \mathcal{R}_L{}' (\mathbf{h}_{r\,i} - \mathbf{b}) - \frac{\mathbf{v}_i}{\|\mathbf{v}_i\|} \|^2$ where $\mathbf{v}_i := \mathbf{S}_L^{-1} \mathcal{R}_L{}' (\mathbf{h}_{r\,i} - \mathbf{b})$. Using simple algebraic manipulation produces the likelihood function (7). □

Optimization tools on Riemannian manifolds are required to solve for the calibration parameters $(\mathcal{R}_L, \mathbf{S}_L, \mathbf{b})$ in the domain Θ, see (Edelman et al., 1998) for a comprehensive introduction to the subject. However, the minimization problem (7) can be formulated on the Euclidean space, which allows for the use of optimization tools for unconstrained problems (Bertsekas, 1999).

Proposition 3. Let $(\mathbf{T}^*, \mathbf{b}_T^*)$ denote the solution of the unconstrained minimization problem

$$\min_{\mathbf{T} \in \mathrm{M}(3), \mathbf{b}_T \in \mathbb{R}^3} \sum_{i=1}^{n} \frac{1}{\sigma^2_{m\,i}} (\| \mathbf{T}(\mathbf{h}_{r\,i} - \mathbf{b}_T) \| - 1)^2 \tag{9}$$

and take the SVD decomposition of $\mathbf{T}^* = \mathbf{U}_T^* \mathbf{S}_T^* \mathbf{V}_T^{*\prime}$, $\mathbf{U}_T \in \mathrm{O}(3)$, $\mathbf{S}_T \in \mathbf{D}^+(3)$, $\mathbf{V}_T \in \mathrm{SO}(3)$. The solution of (7) is given by $\mathbf{R}_L^* = \mathbf{V}_T^*$, $\mathbf{S}_L^* = \mathbf{S}_T^{*\,-1}$, $\mathbf{b}^* = \mathbf{b}_T^*$.

Proof. Using the equality $\| \mathbf{V}_L \mathbf{S}_L^{-1} \mathcal{R}_L' (\mathbf{h}_{r\,i} - \mathbf{b}) \| = \| \mathbf{S}_L^{-1} \mathcal{R}_L' (\mathbf{h}_{r\,i} - \mathbf{b}) \|$ for any $\mathbf{V}_L \in \mathrm{O}(3)$, and the fact that, by the SVD decomposition, $\mathbf{T} := \mathbf{V}_L \mathbf{S}_L^{-1} \mathcal{R}_L'$ is a generic element of M(3), produces the desired results. □

By Proposition 3, the calibration parameters of equation (3) are obtained by solving (9) and decomposing the resulting $\mathbf{T}^*$. Although (9) could be derived using (2), the intermediate derivations (6) and (7) were presented to show that (i) the sensor readings lie on an ellipsoid manifold parametrized by $\mathcal{R}_L$, $\mathbf{S}_L$ and $\mathbf{b}$ (ii) the alignment matrix, represented by $\mathbf{V}_L$ (or $\mathbf{U}_T^*$) cannot be determined in the calibration process, given that there are no body referenced measurements.

In this work, the minimization problem (9) is solved by using the gradient and Newton-descent method for

Euclidean spaces (Bertsekas, 1999), and the Armijo rule for the step size determination. The gradient and Hessian of the log-likelihood function are computed analytically and presented in Appendix B.

Given the calibration parameters $(\mathcal{R}_L, \mathbf{S}_L, \mathbf{b})$, an unbiased and unit norm representation of the Earth magnetic field in the calibration frame $\{C\}$ is obtained by algebraic manipulation of (3), resulting in

$$^{C}\mathbf{h}_i = \mathbf{S}_L^{-1}\mathcal{R}'_L(\mathbf{h}_{r\,i} - \mathbf{b}). \tag{10}$$

A good initial guess of the scaling and bias calibration parameters is produced by the estimator proposed in (Gebre-Egziabher et al., 2006). The locus of measurements described by $\|^{E}\mathbf{h}\|^2 = \|\mathbf{S}^{-1}(\mathbf{h}_r - \mathbf{b})\|^2$ is expanded and, by defining a nonlinear change of variables, it is rewritten as pseudo-linear least squares estimation problem

$$H(\mathbf{h}_r)f(\mathbf{b}, \mathbf{s}) = b(\mathbf{h}_r) \tag{11}$$

where the matrix $H(\mathbf{h}_r) \in \mathrm{M}(n, 6)$ and the vector $b(\mathbf{h}_r) \in \mathbb{R}^n$ are nonlinear functions of the vector readings and the vector of unknowns $f(\mathbf{b}, \mathbf{s}) \in \mathbb{R}^6$ is a nonlinear function of the calibration parameters. The algorithm is found to yield a good first guess of the calibration parameters, and for a detailed description of the terms in (11) the reader is referred to (Elkaim and Foster, 2006).

2.4 Magnetometer Alignment

The representation of $^{B}\mathbf{h}_i$ in the body frame is necessary in attitude determination algorithms (Markley, 1989), however the results of the calibration algorithm provide magnetic readings in the calibration frame, that is $^{C}\mathbf{h}_i$. By means of (4), $^{B}\mathbf{h}_i$ can be obtained if the alignment matrix $\mathbf{V}_L \in \mathrm{O}(3)$ is known.

As illustrated in Fig. 2, two vector readings represented in $\{C\}$ and $\{B\}$ frames are sufficient to characterize a rigid rotation $\mathbf{V}_L \in \mathrm{SO}(3)$, or a rotation with reflection $\mathbf{V}_L \in (\mathrm{O}(3) \setminus \mathrm{SO}(3))$, but the determination of an orthogonal transformation $\mathbf{V}_L \in \mathrm{O}(3)$ requires at least three linearly independent vectors readings. The well known results for the orthogonal Procrustes problem (Gower and Dijksterhuis, 2004) are adopted to determine the sensor alignment.

Theorem 4. (Orthogonal Procrustes Problem). Take two sets of vector readings in $\{C\}$ and $\{B\}$ coordinate frames, concatenated in the form $^{C}\mathbf{X} = \begin{bmatrix} ^{C}\mathbf{h}_1 & \dots & ^{C}\mathbf{h}_n \end{bmatrix}$ and $^{B}\mathbf{X} = \begin{bmatrix} ^{B}\mathbf{h}_1 & \dots & ^{B}\mathbf{h}_n \end{bmatrix}$ where $n \geq 3$. Assume that $^{B}\mathbf{X}^{C}\mathbf{X}'$ is nonsingular, and denote the corresponding SVD as $^{B}\mathbf{X}^{C}\mathbf{X}' = \mathbf{U}\mathbf{\Sigma}\mathbf{V}'$, where $\mathbf{U}, \mathbf{V} \in \mathrm{O}(3)$, $\mathbf{\Sigma} \in \mathrm{D}^{+}(3)$. The optimal orthogonal matrix $\mathbf{V}_L^* \in \mathrm{O}(3)$ that minimizes the transformation from $\{B\}$ to $\{C\}$ coordinates frames in least squares sense, i.e. $\min_{\mathbf{V}_L \in \mathrm{O}(3)} \sum_{i=1}^{n} \|^{C}\mathbf{h}_i - \mathbf{V}'_L\,^{B}\mathbf{h}_i\|^2$, is unique and given by $\mathbf{V}'_L{}^{*} = \mathbf{V}\mathbf{U}'$.

Using (10), the calibrated and aligned magnetic field vector reading is given by

$$^{B}\mathbf{h}_i = \mathbf{V}_L\mathbf{S}_L^{-1}\mathcal{R}'_L(\mathbf{h}_{r\,i} - \mathbf{b}) \tag{12}$$

It is assumed without loss of generality that $^{E}\mathbf{h}$ lies on the unit sphere, and hence the norm scaling factor is incorporated in the scaling matrix $\mathbf{S}_L$. If $\|^{E}\mathbf{h}\| = \alpha, \alpha \neq 1$ is considered, the calibrated sensor reading is given by $^{B}\mathbf{h}_{i\alpha} = \alpha\,^{B}\mathbf{h}_i$.

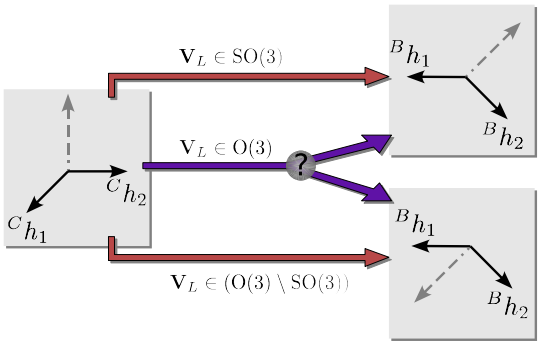

Fig. 2. Alignment ambiguity with two vector readings

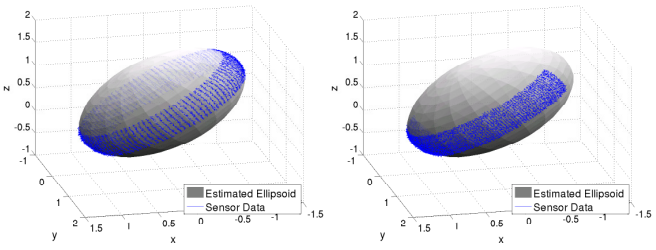

(a) Ring Shaped Data (b) Arch Shaped Data

Fig. 3. Ellipsoid fitting (Simulation Data)

3. ALGORITHM IMPLEMENTATION AND RESULTS

In this section, the proposed methodology is validated using simulated and experimental data from a triad of low-cost magnetometers.

3.1 Simulation Results

The calibration algorithm was first analyzed using simulated data. The reference calibration parameters from (1) are

$$\mathbf{S}_M = \mathrm{diag}(1.2, 0.8, 1.3), \begin{bmatrix}\psi\\ \theta\\ \phi\end{bmatrix} = \begin{bmatrix}2.0\,^{\circ}\\ 1.0\,^{\circ}\\ 1.5\,^{\circ}\end{bmatrix}, \mathbf{b}_{HI} = \begin{bmatrix}-1.2\\ 0.2\\ -0.8\end{bmatrix}\ \mathrm{G},$$

$$\mathbf{b}_M = \begin{bmatrix}1.5\\ 0.4\\ 2.7\end{bmatrix}\ \mathrm{G}, \mathbf{C}_{SI} = \begin{bmatrix}0.58 & -0.73 & 0.36\\ 1.32 & 0.46 & -0.12\\ -0.26 & 0.44 & 0.53\end{bmatrix},$$

and the magnetometer noise, described in the sensor space, is a zero mean Gaussian noise with standard deviation $\sigma_m = 5\,\mathrm{mG}$. The likelihood function f is normalized by the number of samples n and the stop condition of the minimization algorithm is $\|\nabla f|_{\mathbf{x}_k}\| < \varepsilon = 10^{-3}$.

The magnetic field readings are obtained for two specific cases, depicted in Fig. 3, where the sensor ellipsoid is only partially traced due to the maneuverability constraints found in robotic platforms. In the first case, a ring shaped uniform set of points is obtained for a Pitch sweep interval of $\theta \in [-20,\ 20]\,^{\circ}$ and full turns in Yaw. In the second case, the ellipsoid's curvature information is reduced by constraining the Yaw to $\psi \in [-90,\ 90]\,^{\circ}$.

The results of 20 Monte Carlo simulations using 10^4 magnetometer readings are presented in Table 1 and depicted in Fig. 3. Given the large likelihood cost of the noncalibrated data, denoted by $f(\mathbf{x}_{-1})$, the initial condition draws the cost function into the vicinity of the

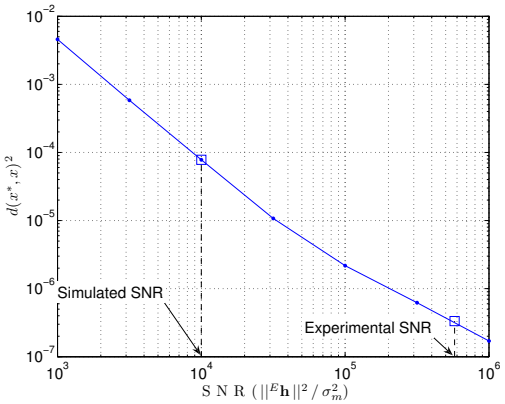

Fig. 4. Estimation Error vs. Signal-to-Noise Ratio (100 MC, Ring Shaped Data)

optimum, and the iterations yield a 20% improvement over the initial guess. The Newton algorithm converges in less iterations than the gradient algorithm, exploiting the second order information of the Hessian, and the execution time is about 5 s in a Matlab 7.3 implementation running on a standard computer with a Pentium Celeron 1.6 Ghz processor.

Defining the distance between the estimated and the actual parameter as $\mathbf{s}_e := \|\mathbf{S}^* - \mathbf{S}\|$,$\mathbf{b}_e := \|\mathbf{b}^* - \mathbf{b}\|$, and $\theta_e := \arccos\left(\frac{\mathrm{tr}(\mathcal{R}^*\mathcal{R}')-1}{2}\right)$, Table 1 shows that the arch shaped data set contains sufficient eccentricity information to estimate the magnetometer calibration parameters. As expected, reducing the information about the ellipsoid curvature slightly degrades the sensor calibration errors.

Although the noise is formulated in the sensor frame, the suboptimal formulation (7) yields accurate results with unitary likelihood weights $\sigma_{m\,i}^2$. Let the distance in the parameter space be given by $d(\mathbf{x}^*,\mathbf{x})^2 := \theta_e^2 + \mathbf{s}_e^2 + \mathbf{b}_e^2$, the influence of the noise power in the estimation error is illustrated in Fig. 4, where the magnetic field magnitude in the San Francisco Bay area is adopted, $\|^E\mathbf{h}\| = 0.5\,\mathrm{G}$.

3.2 Experimental Results

The algorithm proposed in this work was used to estimate the calibration parameters for a set of 6×10^4 points obtained from a Honeywell HMC1042L 2-axis magnetometer and a Honeywell HMC1041Z for the third (Z) axis, sampled with a TI MSC12xx microcontroller with a 24bit Delta Sigma converter, at 100Hz, see (Elkaim and Foster, 2006) for details. A gimbal system was maneuvered to collect (i) a set of sensor readings spanning the ellipsoid surface, Fig. 5(a), (ii) only four ellipsoid sections, Fig. 5(b).

The calibration algorithm converged to a minimum within 60 Newton method iterations, taking less than 40 s. Although the second data set traced a smaller region of the ellipsoid, it was sufficient to characterize the ellipsoid's eccentricity and rotation, as depicted in Fig. 5(b).

Given the calibration parameters, the sensor noise is characterized by rewriting (3) as $\mathbf{n}_{m\,i} = \mathbf{h}_r - (\mathcal{R}_L^*\mathbf{S}_L^{*\,C}\mathbf{h}_i^* + \mathbf{b}^*)$ where ${}^C\mathbf{h}_i^*$ is given in the proof of Proposition 2. The obtained experimental standard deviation of the sensor noise is $\sigma_m = 0.65\,\mathrm{mG}$, which evidences that the signal-

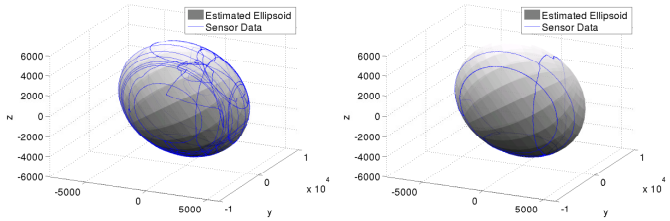

(a) Ellipsoid Surface Data (b) Ellipsoid Sections Data

Fig. 5. Ellipsoid Fitting (Experimental Data)

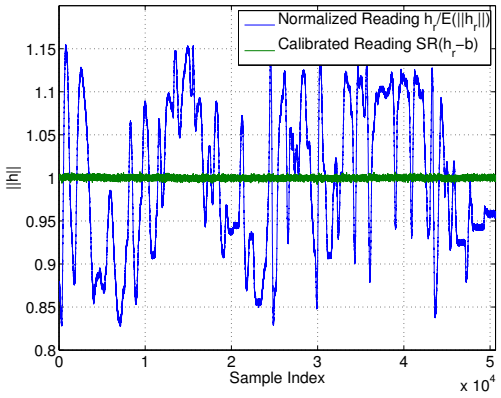

(a) Ellipsoid Surface Data

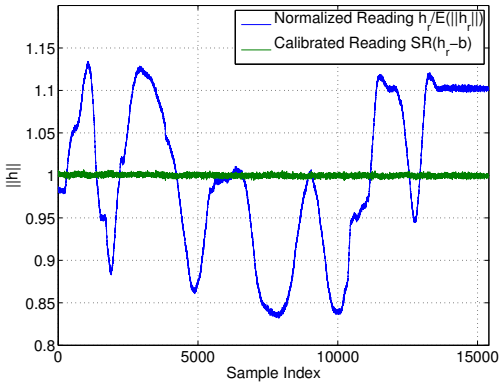

(b) Ellipsoid Sections Data

Fig. 6. Magnetometer Data Fitting

to-noise ratio of a typical low-cost magnetometer is better than that assumed in the simulations of Section 3.1, as depicted in Fig. 4.

The calibrated magnetometer data are compared to the raw data in Fig. 6. The calibrated readings are near to the unit circle locus, which validates the proposed unified error formulation of Theorem 1 and shows that the combined effect of the magnetic distortions is successfully compensated for.

4. CONCLUSIONS

A new estimation algorithm was derived and validated for the onboard calibration of three-axis strapdown magnetometers. An equivalent sensor error model was derived, and it was shown that the nonideal sensor measurements describe an ellipsoid manifold. The parameter optimiza-

Table 1. Calibration Results

		$f(\mathbf{x}_{-1})$	$f(\mathbf{x}_0)$	$f(\mathbf{x}^*)$	iterations	θ_e	$\mathbf{s}_e$	$\mathbf{b}_e$
Gradient Method	Ring Shaped Data	3.28×10^{-1}	1.17×10^{-4}	9.64×10^{-5}	2246	1.74×10^{-3}	7.61×10^{-3}	3.54×10^{-4}
	Arch Shaped Data	4.36×10^{-1}	1.18×10^{-4}	9.62×10^{-5}	1932	1.46×10^{-2}	1.65×10^{-2}	1.74×10^{-2}
Newton Method	Ring Shaped Data	3.28×10^{-1}	1.18×10^{-4}	9.64×10^{-5}	37.0	1.74×10^{-3}	7.61×10^{-3}	3.54×10^{-4}
	Arch Shaped Data	4.37×10^{-1}	1.18×10^{-4}	9.62×10^{-5}	37.2	1.46×10^{-2}	1.65×10^{-2}	1.75×10^{-2}

tion problem was formulated resorting to a Maximum Likelihood Estimator, and an optimization algorithm was derived using the gradient and Newton descent methods. An algorithm to produce good initial conditions was presented. A closed form alignment algorithm was proposed, based on the solution to the orthogonal Procrustes problem. Simulation and experimental results for low-cost sensors show that the proposed algorithm is computationally fast and can be adopted for online calibration in robotic platforms with maneuverability constraints. Future work will include the adaptation of the proposed algorithm to the 2D (heading only) case in marine and land robotic platforms.

REFERENCES

R. Alonso and M.D. Shuster. Complete linear attitude-independent magnetometer calibration. *The Journal of the Astronautical Sciences*, 50(4):477–490, October-December 2002.

D.P. Bertsekas. *Nonlinear Programming*. Athena Scientific, 2nd edition, 1999.

N. Bowditch. *The American Pratical Navigator*. Defense Mapping Agency, 1984.

D. Choukroun, I. Y. Bar-Itzhack, and Y. Oshman. Optimal-request algorithm for attitude determination. *Journal of Guidance, Control, and Dynamics*, 27(3): 418–425, May-June 2004.

J.L. Crassidis, K. Lai, and R.R. Harman. Real-time attitude-independent three-axis magnetometer calibration. *Journal of Guidance, Control, and Dynamics*, 28 (1):115–120, January-February 2005.

W. Denne. *Magnetic Compass Deviation and Correction*. Sheridan House Inc, 3rd edition, 1979.

A. Edelman, T.A. Arias, and S.T. Smith. The geometry of algorithms with orthogonality constraints. *SIAM Journal on Matrix Analysis and Applications*, 20(2): 303–353, 1998.

G.H. Elkaim and C. Foster. Extension of a Non-Linear, Two-Step Calibration Methodology to Include Non-Orthogonal Sensor Axes. IEEE Journal of Aerospace Electronic Systems, Technical Note, submitted August 2006, accepted for publication, 2006.

B. Gambhir. Determination of Magnetometer Biases Using Module RESIDG. Technical Report 3000-32700-01TN, Computer Sciences Corporation, March 1975.

W. Gander, G.H. Golub, and R. Strebel. Least-squares fitting of circles and ellipses. *BIT*, 43:558–578, 1994.

D. Gebre-Egziabher, G.H. Elkaim, J.D. Powell, and B.W. Parkinson. Calibration of Strapdown Magnetometers in Magnetic Field Domain. *ASCE Journal of Aerospace Engineering*, 19(2):1–16, April 2006.

J. C. Gower and G. B. Dijksterhuis. *Procrustes Problems*. Number 30 in Oxford Statistical Science Series. Oxford University Press, USA, 2004.

T. E. Humphreys, M. L. Psiaki, E. M. Klatt, S. P. Powell, and P. M. Kintner, Jr. Magnetometer-based attitude and rate estimation for spacecraft with wire booms. *Journal of Guidance, Control, and Dynamics*, 28(4): 584–593, July-August 2005.

S.M. Kay. *Fundamentals of Statistical Signal Processing: Estimation*. Prentice-Hall, 1993.

F.L. Markley. Attitude determination and parameter estimation using vector observations: Theory. *The Journal of the Astronautical Sciences*, 37(1):41–58, January-March 1989.

Gilbert Strang. *Linear Algebra and Its Applications*. Brooks Cole, 3rd edition, 1988.

Appendix A. EXTERNAL MAGNETIC NOISE

Considering that the main sources of electromagnetic interference are external, the magnetic noise influence in the magnetometer reading can be modeled as

$$\begin{aligned}\mathbf{h}_{r\,i} &= \mathbf{S}_M\mathbf{C}_{NO}(\mathbf{C}_{SI}({}^B_E\mathbf{R}_i{}^E\mathbf{h} + {}^B_N\mathbf{R}\,\mathbf{n}_{m\,i}) + \mathbf{b}_{HI}) + \mathbf{b}_M \\ &= \mathbf{C}^B\mathbf{h}_i + \mathbf{C}^B_N\mathbf{R}\,\mathbf{n}_{m\,i} + \mathbf{b} = \mathcal{R}_L\mathbf{S}_L{}^C\mathbf{h}_i + \mathcal{R}_L\mathbf{S}_L\mathbf{V}'_L{}^B_N\mathbf{R}\,\mathbf{n}_{m\,i} + \mathbf{b}\end{aligned}$$

where ${}^B_N\mathbf{R}$ rotates from the coordinate frame $\{N\}$ where the magnetic noise is defined, to the body coordinate frame. Assuming that $\mathbf{n}_{m\,i}$ is a zero mean Gaussian process with variance $\sigma^2_{m\,i}$, the p.d.f. of each $\mathbf{h}_{r\,i}$ is also Gaussian

$$\mathbf{n}_{m\,i} \sim \mathcal{N}(0, \sigma^2_{m\,i}\mathbf{I}) \Rightarrow \mathbf{h}_{r\,i} \sim \mathcal{N}(\mathcal{R}_L\mathbf{S}_L{}^C\mathbf{h}_i + \mathbf{b}, \sigma^2_{m\,i}\mathcal{R}_L\mathbf{S}^2_L\mathcal{R}'_L).$$

Using the p.d.f. of the $\mathbf{h}_{r\,i}$, straightforward analytical derivations show that MLE formulation is given by (6). The ellipsoid obtained by (6) tends to fit best the points with lower eccentricity, but this effect can be balanced by defining appropriate curvature weights $\sigma^2_{m\,i}$, as convincingly argued in (Gander et al., 1994).

Appendix B. DESCENT METHOD MATRICES

Let $\mathbf{u}_i := \mathbf{h}_{r\,i} - \mathbf{b}$, the gradient of the likelihood function $f := \sum_{i=1}^n \frac{1}{\sigma^2_{m\,i}}(\|\mathbf{T}(\mathbf{h}_{r\,i}-\mathbf{b})\|-1)^2$, is described by $\nabla f|_{\mathbf{x}} = \sum_{i=1}^n \frac{2c_T}{\sigma^2_{m\,i}}\left[(\mathbf{u}_i \otimes (\mathbf{T}\mathbf{u}_i))'\ (-\mathbf{T}'\mathbf{T}\mathbf{u}_i)'\right]'$ where $c_T := 1 - \|\mathbf{T}\mathbf{u}_i\|^{-1}$ and $\otimes$ denotes the Kronecker product. The Hessian $\nabla^2 f|_{\mathbf{x}} = \begin{bmatrix}\mathbf{H}_{\mathbf{T},\mathbf{T}} & \mathbf{H}_{\mathbf{T},\mathbf{b}} \\ \mathbf{H}'_{\mathbf{T},\mathbf{b}} & \mathbf{H}_{\mathbf{b},\mathbf{b}}\end{bmatrix}$ is given by the following submatrices

$$\mathbf{H}_{\mathbf{T},\mathbf{T}} = \sum_{i=1}^n \frac{2}{\sigma^2_{m\,i}}\left[\frac{(\mathbf{u}_i\mathbf{u}'_i)\otimes(\mathbf{T}\mathbf{u}_i\mathbf{u}'_i\mathbf{T}')}{\|\mathbf{T}\mathbf{u}_i\|^3} + c_T\left[(\mathbf{u}_i\mathbf{u}'_i)\otimes\mathbf{I}\right]\right]$$

$$\mathbf{H}_{\mathbf{T},\mathbf{b}} = \sum_{i=1}^n \frac{-2}{\sigma^2_{m\,i}}\left[\frac{(\mathbf{u}_i\otimes\mathbf{T}\mathbf{u}_i)\,\mathbf{u}'_i\mathbf{T}'\mathbf{T}}{\|\mathbf{T}\mathbf{u}_i\|^3} + c_T\,(\mathbf{u}_i\otimes\mathbf{T} + \mathbf{I}\otimes\mathbf{T}\mathbf{u}_i)\right]$$

$$\mathbf{H}_{\mathbf{b},\mathbf{b}} = \sum_{i=1}^n \frac{2}{\sigma^2_{m\,i}}\left[\frac{\mathbf{T}'\mathbf{T}\mathbf{u}_i\mathbf{u}'_i\mathbf{T}'\mathbf{T}}{\|\mathbf{T}\mathbf{u}_i\|^3} + c_T\mathbf{T}'\mathbf{T}\right].$$